Premelting hcp to bcc Transition in Beryllium

Y. Lu, T. Sun, Ping Zhang, P. Zhang, D.-B. Zhang, and R. M. Wentzcovitch

Phys. Rev. Lett. **118**, 145702 — Published 7 April 2017

DOI: 10.1103/PhysRevLett.118.145702

Pre-melting *hcp* to *bcc* Transition in Beryllium

Y. Lu,[1] T. Sun,[2] Ping Zhang,[3] P. Zhang,[4,1] D.-B. Zhang,[1,*] and R. M. Wentzcovitch[5]

[1] *Beijing Computational Science Research Center, Beijing 100193, China*
[2] *Key Laboratory of Computational Geodynamics, University of Chinese Academy of Sciences, Beijing 100049, China*
[3] *Institute of Applied Physics and Computational Mathematics, Beijing 100088, China*
[4] *Department of Physics, University at Buffalo, State University of New York, Buffalo, New York 14260, USA*
[5] *Department of Chemical Engineering and Materials Science, and Minnesota Supercomputing Institute, University of Minnesota, Minneapolis, MN, 55455, USA*

Beryllium (Be) is an important material with wide applications ranging from aerospace components to X-ray equipments. Yet a precise understanding of its phase diagram remains elusive. We have investigated the phase stability of Be using a recently developed hybrid free energy computation method that accounts for anharmonic effects by invoking phonon quasiparticles. We find that the *hcp* $\rightarrow$ *bcc* transition occurs near the melting curve at $0 < P < 11$ GPa with a positive Clapeyron slope of 41 ± 4 K/GPa, which is more consistent with recent experimental measurements. This work also demonstrates the validity of this theoretical framework based on phonon quasiparticle to study structural stability and phase transitions in strongly anharmonic materials.

PACS numbers: 63.20.Ry, 81.30.Bx, 61.50.Ks, 63.20.D-, 64.70.K-

Resolving phase boundaries is challenging for both experimentation and theory given the uncertainties from several sources, especially at very high pressure (P) and high temperature (T). Beryllium (Be) is a typical system whose phase diagram remains an open problem despite intense investigations. It assumes a hexagonal close-packed (*hcp*) structure at relatively low T [1]. However, unlike other metal systems [2], the stability of the body-centered cubic (*bcc*) phase at high T, and the associated *hcp*/*bcc* phase transition are not well understood yet. Be is important for both fundamental research [3–6] and practical applications. Being a strong and light-weight metal, it has been widely used in a broad range of technological applications in harsh environments and extreme PT conditions, e.g., up to $T > 4{,}000$ K and $P > 200$ GPa [7–11].

Equipped with diamond anvil cells (DAC) technique coupled with X-Ray diffraction, recent experimental efforts have made significant progress in understanding the structure and phase stability of Be [12–18]. Lazicki et al. [12] conducted a systematic study of Be covering wide PT ranges: $8 < P < 205$ GPa and $300 < T < 4{,}000$ K [12]. There are also several other experiments conducted at ambient temperature for pressures up to 200 GPa [13, 17]. In these measurements, no sign of *bcc* symmetry was ever captured. In addition, a report from Evans et al. indicates that there is no *bcc* Be for the pressure range of $15 < P < 50$ GPa for temperatures up to 2,000 K (see Ref. [19] for associated discussion). These experimental evidences hint that *bcc* Be is likely to be a high temperature phase within a narrow pressure region at relative low pressures, if it exists at all. Indeed, *bcc* Be was only observed [20] at $T > 1{,}500$ K around ambient pressure before melting (The melting temperature at ambient pressure $T_M \sim 1{,}550$ K). Similar result was reported by Abey [21] by using differential thermal analysis, where the *hcp*/*bcc* phase boundary between $0 < P < 2.5$ GPa is quite near the melting line. On the contrary, through temperature dependent resistance, Francois and Contre inferred that the *hcp*/*bcc* phase boundary between $0 < P < 6$ GPa has a negative Clapeyron slope (-52 ± 8 K/GPa) [22]. According to experimental measurements made by Lazicki et al. [12] and others [13, 17], this result, however, no longer holds. On the theory side, the study of Be's phase diagram using conventional methods encounters significant difficulties. The lattice dynamics of *bcc* Be is highly anharmonic, and the widely used quasi-harmonic approximation (QHA) and Debye model are not able to capture such effect [19, 23–28]. For this reason, theoretical study of *bcc* Be and the associated *hcp*/*bcc* phase transition is missing for $P < 11$ GPa (density $< 2.1 g/cc$) where *bcc* Be is dynamically unstable at 0 K [24]. At $P > 11$ GPa, *bcc* Be is dynamically stabilized by pressure and the QHA might, in principle, be applied. However, the *hcp*/*bcc* boundary [23–25] predicted by the QHA does not agree with experiments [12], suggesting that anharmonic effects still play an important role at higher pressures.

In this Letter, we report a new investigation of the phase stability of *bcc* Be and the associated *hcp* $\rightarrow$ *bcc* phase transition boundary up to 30 GPa and temperatures up to 2,000 K. We have used a recently developed hybrid approach [29, 30] that combines first-principles molecular dynamics (MD) and lattice dynamics calculations to address anharmonic effects in the free energy. In this method, the concept of phonon quasiparticles offers a quantitative characterization of the effects of lattice anharmonicity [31, 32]. We show that Be exhibits pronounced anharmonic effects in both the *bcc* and *hcp* phases. Specifically, our results reveal the dynamical sta-

bilization of *bcc* Be with increasing T. The *bcc* phase, however, is favorable only in a narrow temperature range near T_M, with *hcp* → *bcc* phase boundary having a positive Clapeyron slope of 41 ± 4 K/GPa. The *bcc* stability field shrinks with increasing pressure and eventually disappears at around 11 GPa. This result agrees overall with experiments [12–18, 20, 21] and differs from other *hcp*/*bcc* phase boundaries (e.g., Mg [33]), usually displaying a negative Clapeyron slope.

In the present approach, phonon quasiparticles are numerically characterized by the mode projected velocity autocorrelation function [29, 30],

$$\langle \mathbf{V}(0) \cdot \mathbf{V}(t) \rangle_{q,s} = \lim_{t_0 \to \infty} \frac{1}{t_0} \int_0^{t_0} \mathbf{V}^*_{q,s}(t') \cdot \mathbf{V}_{q,s}(t'+t) dt', \tag{1}$$

where $\mathbf{V}_{q,s}(t) = \sum_{i=1}^{N} \sqrt{M_i} v(t) \cdot \hat{\epsilon}^i_{q,s} \exp(i\mathbf{q} \cdot \mathbf{R}_i)$ is the mode projected and mass weighted velocity for normal mode (q, s) with wave vector $\mathbf{q}$; $v_i(t)(i = 1, ..., N)$ is the atomic velocity produced by first-principles MD simulations with N atoms, and M_i and $\mathbf{R}_i$ are the atomic mass and coordinate of atom i, respectively. $\hat{\epsilon}^i_{q,s}(i = 1, ..., N)$ is the polarization vector of normal mode (q, s) calculated using density functional perturbation theory (DFPT) [34]. For a well-defined phonon quasiparticle, the velocity autocorrelation function displays an oscillatory decaying behavior and its Fourier transform, i.e., the power spectrum,

$$G_{q,s} = \int_0^{\infty} \langle \mathbf{V}(0) \cdot \mathbf{V}(t) \rangle_{q,s} \exp(i\omega t) dt, \tag{2}$$

should have a Lorentzian-type line shape [29, 30]. The renormalized phonon frequency $\widetilde{\omega}_{q,s}$, and the linewidth, $\Gamma_{q,s}$ can then be obtained as discussed in more details in the Supplemental Materials.

The concept of phonon quasiparticle reduces the complex problem of interacting anharmonic phonons to an effective non-interacting system [31], such that the conventional kinetic gas model and, to a great extent, the theory of harmonic phonons are still applicable. Moreover, since structural phase transition is triggered by lattice vibrations for many cases, insight into the transition mechanism can be also obtained by monitoring the variation of frequencies and line widths of phonon quasiparticles.

We used the Vienna *ab initio* simulation package (VASP) [36, 37] to carry out first principles MD simulations on $4 \times 4 \times 4$ supercells (128 atoms) of Be. We used the generalized gradient approximation of Perdew, Burke, and Ernzerhof [38] and the projector-augmented wave method [35] with an associated plane-wave basis set energy cutoff of 350 eV. For metallic Be, the finite temperature Mermin functional [46, 47] was used. Simulations were carried out at a series of volumes (V): $6.21 < V < 8.71$Å^3/atom for *bcc* Be and $6.35 < V <$ 8.83Å^3/atom for *hcp* Be. For *hcp* Be, proper aspect ratio (c/a) is adopted to obtain good hydrostatic conditions for specific volume and temperature. Temperatures ranging from 300 to 2,800 K are controlled through the Nosé dynamics [40]. The considered volumes and temperatures result in a pressure range of $0 < P < 30$ GPa. For each volume and temperature, multiple independent MD runs (5 parallel replica) were performed to improve phase space sampling quality that also allow for evaluation of statistical uncertainties. Each MD run lasted 50 ps and used a time step of 1 fs. Harmonic phonon frequencies and normal modes were calculated using density functional perturbation theory (DFPT) [34].

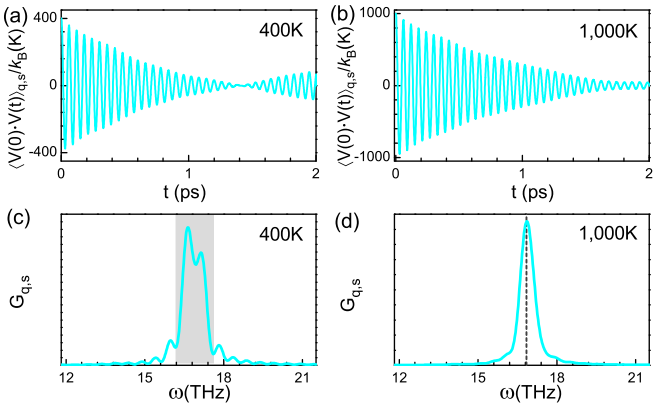

FIG. 1. Mode projected velocity auto-correlation functions of the TA1 acoustic mode (q, s) at $\mathbf{q} = N$ with a harmonic frequency of 18.2 THz of *bcc* Be at (a) 400 K and (b) 1,000 K, respectively. (c) and (d) show the corresponding power spectra. In (c), the shaded area between 16.2 THz and 17.6 THz covers two major peaks, indicating the breakdown of the phonon quasiparticle picture. In (d), the vertical dashed line at 16.8 THz indicates the frequency of the well-defined phonon quasiparticle.

Before proceeding, we should clarify the general understanding of the *hcp* → *bcc* transition. The low T and low P *hcp* structure relates to the *bcc* structure through the zone center transverse optical (TO) mode and a macroscopic strain. This mode consists of opposite displacements of neighboring (0001) planes along ⟨1010⟩ and softens with increasing T. This is not necessarily a soft mode transition, but generally a first order transition with negative Clapeyron slope [33]. The (0001) plane transforms into the (110) plane of the *bcc* phase. This picture was validated by an early variable cell shape molecular dynamics study [44]. The opposite *bcc* → *hcp* transition involves the lowest transverse acoustic mode (TA2) at $\mathbf{q} = [1/2, 1/2, 0]$, the N point of the Brillouin zone, marked by an open circle in Fig. 2(a). With this in mind we monitor closely the behavior of these modes with changing T.

We first investigate the behavior of phonon quasiparticles at different temperatures. For *bcc* Be, phonon quasi-

particles are not well defined at low T as found in other systems [31], but recovered at high T for unstable (soft) modes e.g., TA2. The analysis of this mode is shown in Fig. S2 of the Supplementary material. It is more interesting to notice that at low T, phonon quasiparticles are not well defined even for certain stable modes with positive harmonic frequencies. Fig. 1 shows $\langle \mathbf{V}(0) \cdot \mathbf{V}(t) \rangle_{q,s}$ and the corresponding power spectra of the TA1 phonon mode at N calculated at 400 K (Fig. 1(a)) and 1,000 K (Fig. 1(b)). This mode is marked by an open square in Fig. 2(a). Although $\langle \mathbf{V}(0) \cdot \mathbf{V}(t) \rangle_{q,s}$ at 400 K displays an oscillatory behavior, the amplitude decay is non-monotonic (Fig. 1(a)). Consequently, the power spectrum has two major peaks within the shaded area as shown in Fig. 1(c). This indicates that the frequency of this mode cannot be well constrained, or equivalently, the corresponding phonon quasiparticle is not well-defined. In contrast, at 1,000 K $\langle \mathbf{V}(0) \cdot \mathbf{V}(t) \rangle_{q,s}$ exhibits a nicely decaying oscillatory behavior, Fig. 1(b). The corresponding power spectrum now has a well-defined Lorentzian line shape with a single and well defined peak, Fig. 1(d). It is thus straightforward to identify the renormalized frequency of this mode as 16.8 THz. Similarly, all other quasiparticle mode frequencies sampled by the 4x4x4 supercell are equally well defined. As previously indicated [29, 30], these renormalized phonon frequencies plus the normal modes enable the calculation of the renormalized force constant matrix and complete phonon dispersions. This quantitative characterization of phonon quasiparticles and renormalized phonon dispersion provide a solid foundation for studying thermal properties.

Figure 2(a) compares the anharmonic phonon dispersion of *bcc* Be at 1,000 K with the harmonic phonon dispersion calculated using DFPT. Results are obtained at the static equilibrium volume of *bcc* Be, 7.81Å^3/atom. There are noticeable differences between the anharmonic and harmonic phonon dispersions. In particular, the unstable (soft) TA2 branch along the $\Gamma - N$ line stabilizes when high temperature anharmonic effects are accounted for. This indicates that *bcc* Be is stabilized by anharmonic effects. To gain further insight into anharmonic effects, we analyze T-dependent phonon frequency shifts. Fig. 2(c) shows that the frequency of the *bcc* zone edge phonon mode at $\mathbf{q} = N$ associated with the TA2 branch calculated at fixed volume varies non-linearly with T. Lowest order many-body perturbation theory (MBPT) [41] predicts a linear frequency shift with T. Therefore, as expected, higher order anharmonic effects ignored in the perturbative treatment play an important role here.

The calculated anharmonic phonon dispersion over the whole Brillouin zone makes it possible to calculate the free energy in the thermodynamic limit ($N \to \infty$). Since *hcp* Be is stable at low T for the entire pressure range of interest, the lattice thermal properties have been studied within the QHA [23–25] without further examination of the validity of the approximation. This naturally brings up a question: how important are anharmonic effects in the free energy in this seemingly stable structure? Fig. 2(b) compares the anharmonic phonon dispersion at $T = 1,000$ K and the harmonic phonon dispersion of

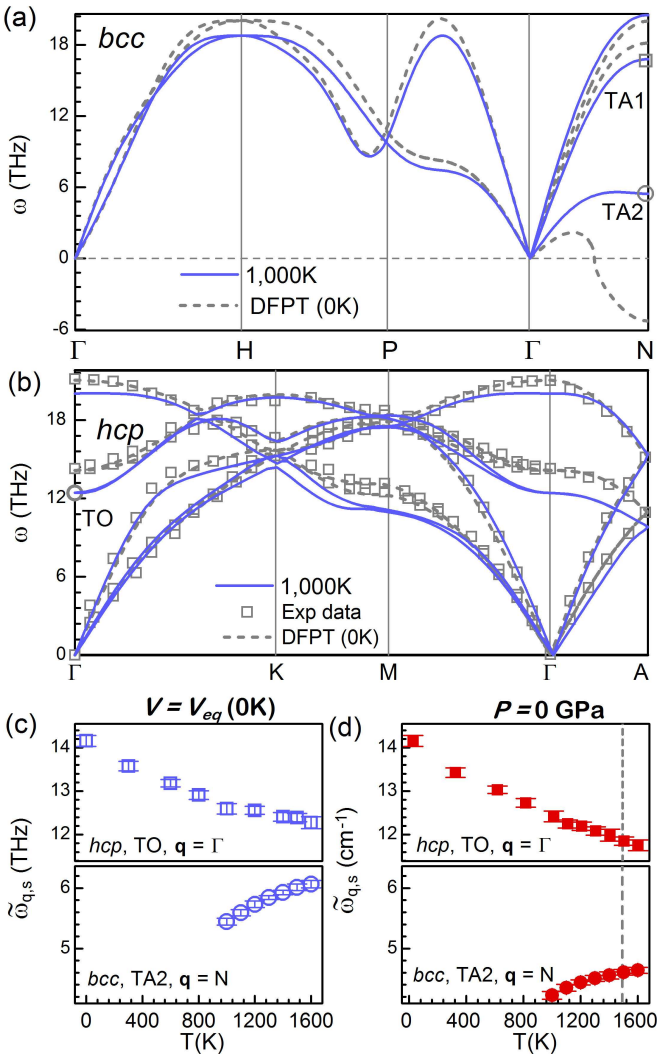

FIG. 2. (a) Anharmonic phonon dispersion at 1,000 K (blue solid curves) and harmonic phonon dispersion calculated using DFPT (grey dashed curves) both at V = 7.81Å^3/atom, the static *bcc* Be equilibrium volume. The two transverse branches are labeled TA1 and TA2, respectively. (b) Anharmonic phonon dispersion calculated at 1,000 K (blue solid curves) and harmonic phonon dispersion calculated using DFPT (grey dashed curves) both at $V = 7.89$Å^3/atom, the static *hcp* Be equilibrium volume. The experimental data is shown for comparison [48]. (c) Temperature dependent frequency shifts of the TA2 $\mathbf{q}$ = N mode [open circle in (a)] and of the TO $\mathbf{q} = \Gamma$ mode [open circle in (b)] calculate at constant volume and (d) at constant zero pressure. The procedure to convert from constant volume to constant pressure was described in [29]. The vertical dashed line in (d) indicates the *hcp*/*bcc* transition temperature.

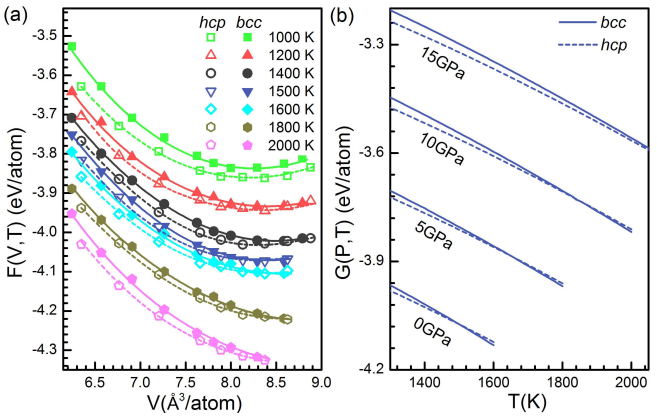

FIG. 3. (a) Free energy $F(V,T)$ versus volumes of Be for *bcc* (solid symbols) and *hcp* (opened symbols) phases at different temperatures. (b) Free energy $G(P,T)$ versus temperature of Be for *bcc* (solid lines) and *hcp* (dashed lines) phases at different pressures. In (a) and (b), the error bars are too small to be visible.

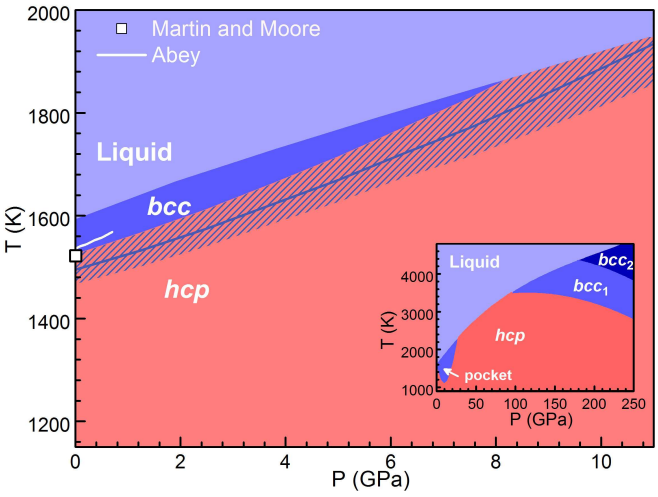

FIG. 4. Phase diagram of Be. The shaded area indicates the uncertainty of our predicted hcp/bcc boundary. The melting line is adopted from Robert et al. [24]. The measured *hcp*/*bcc* phase boundary (solid line [21]) and the experimental point for *bcc* Be (opened square) [20] are shown for comparison. The insert summarizes the phase diagram of Be as predicted by previous theoretical studies: *hcp*/*bcc*$_1$ and the pocket at relative low pressure zone [24], and *hcp*/*bcc*$_2$ [19].

hcp Be calculated at a fixed volume of 7.89Å^3/atom corresponding to zero static pressure. The differences, although not alarming, are still significant in most of the Brillouin zone. A detailed analysis of individual phonon modes in the Supplementary material reveals that the frequency shifts with increasing T can be positive, negative or nearly zero, demonstrating the complexity of lattice anharmonic effects. What is important here is that the large frequency shifts in *hcp* Be should be incorporated into the free energy calculation for more accurate evaluations of thermodynamic properties and phase boundaries.

The large frequency shifts not only reveal pronounced anharmonic effects but also shed light on the microscopic mechanism of this phase transition. As mentioned earlier, the *hcp* and *bcc* structures are related by a combination of phonon displacements and a macroscopic strain [42]. Together they provide a path for the *hcp* $\rightarrow$ *bcc* transition. The frequency of the zone center TO mode drops significantly from 14.2 to 12.3 Thz when T increases from 0 to 1,600 K (see Fig. 2(c)). This observation is consistent with expectations based on the anticipated transformation mechanism [33, 43, 44]. We note that although the frequency shift is very large at 1,600 K, the picture of phonon quasiparticle is still valid for the *hcp* phase (see the Supplementary material for detailed analysis). As mentioned earlier, from the Brillouin zone-folding relation, the corresponding mode in *bcc* Be is the zone edge TA2 mode at $\mathbf{q} = N$, whose property is shown in Fig. 2(c) and (d).

We now demonstrate that anharmonic effects are critical for obtaining this *hcp* $\rightarrow$ *bcc* phase boundary. When using anharmonic T-dependent phonon dispersions, the QHA free energy formula is no longer valid whereas the entropy formula is still applicable [45]. Therefore, we first calculate the vibrational entropy [29, 31],

$$S_{vib} = k_B \sum_{\mathbf{q}s} [(n_{\mathbf{q}s}+1)\ln(n_{\mathbf{q}s}+1) - n_{\mathbf{q}s}\ln n_{\mathbf{q}s}], \quad (3)$$

with $n_{\mathbf{q}s} = [\exp(\hbar\tilde{\omega}_{\mathbf{q},s}/k_BT)-1]^{-1}$, and obtain the total free energy as:

$$F(V,T) = F(V,T_0) - \int_{T_0}^{T} S(T')dT'. \quad (4)$$

where T_0 is 1,000 K, S is the total entropy including both vibrational and electronic contributions (See the Supplementary material for more details). Our analysis of phonon quasiparticles demonstrates that they are well defined for both phases for $T \geq 1,000$ K, therefore the choice of T_0. $F(V,T_0) = E(V,T_0) + T_0S(V,T_0)$, where $E(V,T_0)$ is the internal energy obtained from the MD simulation. Fig. 3(a) displays the calculated free energies for both *bcc* and *hcp* phases. It is seen that at $T \geq 1,200$ K, $V_{bcc} > V_{hcp}$, and consistently, the common tangent to these curves starts to have negative slope, indicating a transition from *hcp* to *bcc* at positive pressure. We note that the volumetric variations of both phases also provide clues to understand the predicted *hcp*/*bcc* transition at very high P (e.g., 400 GPa) [23–25]. More details of the variation of V_{bcc} and V_{hcp} is shown in Fig. S6 the Supplementary material.

It is more convenient to convert $F(V,T)$ into $G(P,T) = F(V,T) + P(V,T)V$ to obtain the phase boundary (see the Supplementary material for details). Fig. 3(b) displays $G(P,T)$ for both *bcc* and *hcp* phases. At each

P, the intersection of G_{bcc} and G_{hcp} gives the *hcp*/*bcc* transition temperature. The resulting *hcp* $\rightarrow$ *bcc* phase boundary shown in Fig. 4 together with the predicted/measured melting line, reveal several important aspects: (i) *bcc* Be is stable only when T approaches the melting point ($T_M \sim 1550$ K at ambient pressure), and the *hcp* $\rightarrow$ *bcc* phase transition occurs only in a narrow pressure range of $0 < P < 11 \pm 2$ GPa. The uncertainty in the transition pressure can be understood from the uncertainties of calculated free energy. From the five parallel replica of BOMD simulations, five different renormalized phonon frequencies $\tilde{\omega}_{q,s}$ are obtained, enabling the estimation of uncertainty of $\tilde{\omega}_{q,s}$ and thus the uncertainty in the free energy, ΔF_{vib}. For example, $\Delta F_{vib} \approx 3.5$ meV/atom in *bcc* Be at 2,000 K with a volume of $V = 7.81 \mathring{A}^3$/atom. The non-negligible ΔF_{vib} for both *hcp* and *bcc* phases brings out an uncertainty in *hcp*/*bcc* phase boundary. At $P = 11$ GPa, this uncertainty is about ± 2 GPa. A detailed analysis of the phase boundary uncertainty is shown in the Supplementary material. We indicate that the obtained transition pressure range within uncertainty is consistent with recent experimental measurements [12, 14–18]. For example, Lazicki et al. [12] inspected the structure of Be for high pressure $P = 205$ GPa at temperature up to $4,000$ K, and for low pressure down to $P = 8$ GPa at temperature up to $1,225$ K and found no sign of *bcc* Be. Our results are also agreement with earlier experiment where *bcc* Be was observed at $T > 1500$ K [20] at ambient pressure. Here it is worth noting that this measurement [20] might not be of sufficient accuracy due to the impurities contained in the samples. (ii) The *hcp*/*bcc* phase boundary has a positive Clapeyron slope of 41 ± 4 K/GPa, as recently suggested [12]. Besides, our predicted Clapeyron slope is close to the experimental value (43 ± 7 K/GPa) reported by Abey [21]. We note that Abey indicated that the *hcp*/*bcc* boundary disappears at a triple point $P = 2.5$ GPa, quite different from out prediction (11 ± 2 GPa). The main reason is that our predicted *hcp*/*bcc* transition temperature is lower than Abey's while the melting line predicted by Robert et al. is higher than Abey's. (iii) Our prediction for the *bcc* stability field does not look like a pocket, as recently suggested, but it does overlap with the PT range of that pocket [24] (see Fig. 4).

In summary, using the concept of phonon quasiparticle, we have investigated the *hcp* $\rightarrow$ *bcc* phase boundary of Be. We find that *bcc* Be is stabilized at low pressures and high temperatures by anharmonic effects. For *hcp* Be, anharmonic effects on phonon properties are also significant. Using anharmonic phonon dispersions, we evaluated the free energies of both phases and showed that the *bcc* phase emerges as a pre-melting phenomenon at relatively low pressures. Our results for the *hcp* $\rightarrow$ *bcc* phase boundary are consistent with most experimental observations [12, 14–18, 20, 21] in all important aspects.

This work was supported by NSFC under Grant Nos. U1530401, 41474069 and 11328401, and NSAF under Grant No. U1530258. RW was supported by the Hareaus visiting professorship award from the University of Frankfurt and by NSF grants EAR-1319368 and -1348066. PZ was supported by the NSF grant DMR-1506669. Computations were performed at Beijing Computational Science Research Center and Minnesota Supercomputing Institute.

* Corresponding author; dbzhang@csrc.ac.cn

[1] J. F. Cannon, *J. Phys. Chem. Ref. Data*, **3**, 781 (1974).
[2] K. Persson, M. Ekman, V. Ozoliņš, *Phys. Rev. B*, **61**, 11221 (2000).
[3] S. H. Glenzer, G. Gregori, R.W. Lee, F. J. Rogers, S.W. Pollaine, and O. L. Landen, *Phys. Rev. Lett.* **90**, 175002 (2003).
[4] S. H. Glenzer, O. L. Landen, P. Neumayer et al., *Phys. Rev. Lett.* **98**, 065002 (2007).
[5] H. J. Lee, P. Neumayer, J. Castor et al., *Phys. Rev. Lett.* **102**, 115001 (2009).
[6] I. Vobornik, J. Fujii, M. Hochstrasser et al., *Phys. Rev. Lett.* **99**, 166403 (2007)
[7] S. W. Haan *et al.*, *Phys. Plasmas* **18**, 051001 (2011).
[8] D. Swift, D. Paisley, and M. Knudon, *AIP Conf. Proc.* **706**, 119 (2003).
[9] K. L. Wilson, R. A Causey, W. L. Hsu, B. E. Mills, M. F. Smith, and J. B. Whitley, *J. Vac. Sci. Technol. A* **8**, 1750 (1990).
[10] D. S. Clark, S.W. Haan, and J. D. Salmonson, *Phys. Plasmas* **15**, 056305 (2008).
[11] D. C. Wilson, P. A. Bradley, N. M. Hoffman *et al.*, *Phys. Plasmas* **5**, 1953 (1998); J. L. Kline, S. A. Yi, A. N. Simakov *et al.*, *Phys. Plasmas* **23**, 056310 (2015).
[12] A. Lazicki, A. Dewaele, P. Loubeyre, and M. Mezouar, *Phys. Rev. B* **86**, 174118 (2012).
[13] W. J. Evans, M. J. Lipp, H. Cynn, C. S. Yoo, M. Somayazulu, D. Häusermann, G. Shen and V. Prakapenka, *Phys. Rev. B* **72**, 094113 (2005).
[14] L. C. Ming and M. H. Manghnani, *J. Phys. F: Met. Phys.* **14**, L1 (1984).
[15] V. Vijayakumar, B. K. Godwal, Y. K. Vohra, S. K. Sikka, and R. Chidambaram, *J. Phys. F: Met. Phys.* **14**, L65 (1984).
[16] A. R. Marder, *Science* **142**, 664 (1963).
[17] K. Nakano, Y. Akahama, and H. Kawamura, *J. Phys.: Condens. Matter.* **14**, 10569 (2002).
[18] N. Velisavljevic, G. N. Chesnut, Y. K. Vohra, S. T. Weir, V. Malba, and J. Akella, *Phys. Rev. B* **65**, 172107 (2002).
[19] L. X. Benedict, T. Ogitsu, A. Trave, C. J. Wu, P. A. Sterne, and E. Schwegler, *Phys. Rev. B* **79**, 064106 (2009).
[20] A. J. Martin and A. Moore, *J. Less-Common Met.* **1**, 85 (1959).
[21] A. Abey, National Technical Reports Library, NTIS Issue Number 198506 (1984).
[22] M. Francois and M. Contre, in *Proceedings of the Conference internationale sur la metallurgie du beryllium*, Grenoble, (Presses Universitaires de France, Paris, 1965).

[23] G. Robert and A. Sollier, *J. Phys. IV France* **134**, 257 (2006).
[24] G. Robert, P. Legrand, and S. Bernard, *Phys. Rev. B* **82**, 104118 (2010).
[25] F. Luo, L.-C. Cai, X.-R. Chen, F.-Q. Jing, and D. Alfé, *J. Appl. Phys.* **111**, 053503 (2012).
[26] G. V. Sin′ko and N. A. Smirnov, *Phys. Rev. B* **71**, 214108 (2005).
[27] K. Kádas, L. Vitos, R. Ahuja, B. Johansson, and J. Kollár, *Phys. Rev. B* **76**, 235109 (2007).
[28] K. Kádas, L. Vitos, B. Johansson, and J. Kollár, *Phys. Rev. B* **75**, 035132 (2007).
[29] D.-B. Zhang, T. Sun, and R. M. Wentzcovitch, *Phys. Rev. Lett.* **112**, 058501 (2014).
[30] T. Sun, D.-B. Zhang, and R. M. Wentzcovitch, *Phys. Rev. B* **89**, 094109 (2014).
[31] T. Sun, X. Shen, and P. B. Allen, *Phys. Rev. B* **82**, 224304 (2010).
[32] A. J. C. Ladd, B. Moran, and W. G. Hoover, *Phys. Rev. B* 34, 5058 (1986).
[33] J. D. Althof, P. B. Allen, R.. M. Wentzcovitch, and J. A. Moriarty, *Phys. Rev. B* **48**, 13253 (1993).
[34] S. Baroni, S. D. Gironcoli, A. D. Corso, and P. Giannozzi, *Rev. Mod. Phys.* **73**, 515 (2001); Giannozzi, et al., *J. Phys. Condens. Matter* **21**, 395502 (2009).
[35] P. E. Blöchl, Phys. Rev. B **50**, 17953 (1994).
[36] G. Kresse, J. Furthmöller, *Phys. Rev. B* **54**, 11169 (1999).
[37] G. Kresse and J. Hafner, *Phys. Rev. B* 49, 14251 (1994).
[38] J. P. Perdew, K. Burke, M. Ernzerhof, *Phys. Rev. B* **77**, 3865 (1996).
[39] A. Togo and I. Tanaka, *Scr. Mater.*, **108**, 1 (2015).
[40] S. Nosé, *J. Chem. Phys.* 81, 511 (1984); W.G. Hoover, *Phys. Rev. A* **31**, 1695 (1985).
[41] A. A.Maradudin and A. E. Fein, *Phys. Rev.* **128**, 2589 (1962).
[42] G. Grimvall, B. Magyari-Koῤe, Vidvuds Ozoliņš, and K. A. Persson, *Rev. Mod. Phys.* **84**, 945 (2012).
[43] R. M. Wentzcovitch and M. L. Cohen, *Phys. Rev. B*, **37**, 5571 (1988).
[44] R. M. Wentzcovitch, *Phys. Rev. B* **50**, 10358 (1994).
[45] D. C. Wallace, *Thermodynamics of Crystals* (Wiley, New York, 1972).
[46] N. D. Mermin, *Phys. Rev.* **137**, A1441 (1965).
[47] R. M. Wentzcovitch, J. L. Martins, and P. B. Allen, *Phys. Rev. B* **45**, 11372 (1992).
[48] R. Stedman, Z. Amilius, R. Pauli, and O. Sundin, J. Phys. F: Met. Phys. **6**, 157 (1976).